Hyperforin Inhibits Cancer Invasion and Metastasis

1. Massimo Donà [1] ,
2. Isabella Dell'Aica [1] ,
3. Elga Pezzato [1] ,
4. Luigi Sartor [1] ,
5. Fiorella Calabrese [2] ,
6. Mila Della Barbera [2] ,
7. Arianna Donella-Deana [3] ,
8. Giovanni Appendino [4] ,
9. Anna Borsarini [5] ,
10. Rosy Caniato [5] , and
11. Spiridione Garbisa [1]

1. *Departments of [1] Experimental Biomedical Sciences, [2]Pathology, and [3]Biological Chemistry, Medical School of Padova; [4]DISCAFF, University of Piemonte Orientale, Novara; and [5]Department of Biology, University of Padova, Padova, Italy*

Abstract

Hyperforin (Hyp), the major lipophilic constituent of St. John's wort, was assayed as a stable dicyclohexylammonium salt (Hyp-DCHA) for cytotoxicity and inhibition of matrix proteinases, tumor invasion, and metastasis. Hyp-DCHA triggered apoptosis-associated cytotoxic effect in both murine (C-26, B16-LU8, and TRAMP-C1) and human (HT-1080 and SK-N-BE) tumor cells; its effect varied, with B16-LU8, HT-1080, and C-26 the most sensitive (IC_{50} = 5 to 8 μmol/L). At these concentrations, a marked and progressive decline of growth was observed in HT-1080 cells, whereas untransformed endothelial cells were only marginally affected. Hyp-DCHA inhibited in a dose-dependent and noncompetitive manner various proteinases instrumental to extracellular matrix degradation; the activity of leukocyte elastase was inhibited the most (IC_{50} = 3 μmol/L), followed by cathepsin G and urokinase-type plasminogen activator, whereas that of the matrix metalloproteinases (MMPs) 2 and 9 showed an IC_{50} > 100 μmol/L. Nevertheless, inhibition of extracellular signal-regulated kinase 1/2 constitutive activity and reduction of MMP-2 and MMP-9 secretion was triggered by 0.5 μmol/L Hyp-DCHA to various degrees in different cell lines, the most in C-26. Inhibition of C-26 and HT-1080 cell chemoinvasion (80 and 54%, respectively) through reconstituted basement membrane was observed at these doses. Finally, in mice that received i.v. injections of C-26 or B16-LU8 cells, daily i.p. administration of Hyp-DCHA—without reaching tumor-cytotoxic blood levels—remarkably reduced inflammatory infiltration, neovascularization, lung weight (−48%), and size of experimental metastases with C-26 (−38%) and number of lung metastases with B16-LU8 (−22%), with preservation of apparently healthy and active behavior. These observations qualify Hyp-DCHA as an interesting lead compound to prevent and contrast cancer spread and metastatic growth.

INTRODUCTION

The use of St. John's wort (*Hypericum perforatum* L., Guttiferae) has its origins in Western medical traditions well before the 1600s. Spurred by the results of controlled but limited trials showing that mild to moderate depression can benefit from oral administration of extracts from this plant, the NIH launched in March 2003 a large-scale clinical trial to determine how the herbal agent fits into the overall management of the disorder and confirm its efficacy. 6

St. John's extracts are a rich source of unique natural products, and the prenylated acylphloroglucinol hyperforin (Hyp) has emerged as key player for the antidepressant activity of the plant (1) , as well as for its severe interactions with several prescription drugs (2) . Although the antidepressant target of Hyp has thus far remained elusive, this compound turned out to be the most powerful ligand ever discovered for the pregnane-X-receptor (3) , a nuclear transcription factor underlying the activation of the P450 cytochrome system, and serving as a xenobiotic sensor to preserve chemical homeostasis.

Hyp was first isolated in the 1960s for its remarkable antibiotic activity against several Gram-positive bacteria, including meticillin-resistant *Staphylococcus aureus* (4) but was later shown to exert also a dose-dependent antiproliferative effect *in vitro* in phytohemagglutinin-stimulated peripheral blood lymphocytes (5) , as well as in several tumor cell lines. Inhibition of proliferation has been reported also *in*

vivo (6) , and the cytotoxic effect of Hyp on human malignant cells was correlated with the induction of caspase-driven apoptosis (7) . This finding could be of great oncological relevance, but no study has yet validated Hyp as an anticancer lead by demonstration of its effectiveness against invasive and metastatic aggressiveness.

Cell invasion and metastasis are critical targets for therapeutic treatment of malignant solid tumors. One key mechanism involved in these pathological processes is the degradation of mechanical barriers represented by specialized extracellular matrices. Tools of election have been found to be some tumor-cell-associated proteinases such as matrix metalloproteinases (MMPs) 2 (8) and 9 (9) ; their expression and activity against matrix macromolecules have been linked to the development of malignant phenotype (10) and shown to overbalance their endogenous inhibitors (*e.g.*, tissue inhibitor of metalloproteinases, α2-macroglobulin, α1-protease inhibitor; ref. 11).

In animal models, generic MMP inhibitors prevent tumor dissemination and formation of metastases (12) ; the possibility of boosting the natural protection against excessive proteolytic activities with designer drugs has led to development of a number of synthetic inhibitors, mainly against MMPs. However, when assayed into clinical trial, these compounds failed to live up to expectations, mostly because of their systemic toxicity (13) .

Certain plant compounds can exert antitumor growth, antiangiogenic, anti-invasive, and antimetastatic effects without apparent toxicity (14, 15, 16, 17) , and (-)epigallocatechin-3-gallate, the major flavonoid contained in green tea, has been found to be a good inhibitor of MMP-2 and MMP-9 (18) , macrophage metalloelastase MMP-12 (19) , and leukocyte serin-elastase (LE; ref. 20). Although a full assessment of the clinical potential of these compounds is not yet possible and must await clarification of issues like absorption, bioavailability, and metabolic fate (21) , the pharmacokinetics of Hyp has been thoroughly investigated, revealing that the compound is available upon oral ingestion, with antidepressive therapeutic doses of St. John's wort leading to serum levels of Hyp reaching 0.45 μmol/L (22) .

Encouraged by these findings, we decided to investigate whether, at these concentrations, Hyp could also be useful in an oncological context, exerting anti-invasive and antimetastatic properties predictive of clinical translation. Hyp, a mixture of interconverting tautomers, is prone to air oxidation and unstable in most organic solvents. Its stable and crystalline dicyclohexylammonium salt (Hyp-DCHA; Fig. 1 ⇓ ; refs. 23 , 24) is a convenient storage form of the natural product already used in studies of antidepressant activity in rats (25) and, for this reason, was chosen for our investigation.

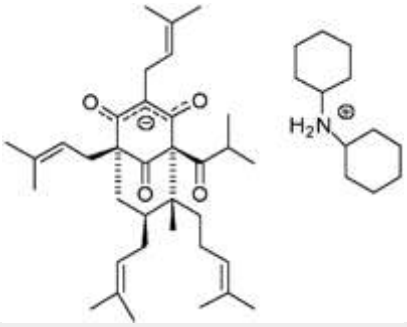

Fig. 1.

Chemical structure of Hyp-DCHA.

MATERIALS AND METHODS

Reagents

Elastase and cathepsin G from human leukocytes, urokinase plasminogen activator (uPA) from human kidney cells, and elastase substrate *N*-methoxysuccinyl-ala-ala-pro-val-*p*-nitroanilide were purchased from Sigma Chemical Co. (St. Louis, MO). Thrombin from human plasma, cathepsin G substrate suc-ala-ala-pro-phe-*p*NA, thrombin substrate H-sar-pro-arg-*p*NA, and uPA substrate Z-val-gly-arg-*p*NA were obtained from Calbiochem-Novabiochem (Nottingham, United Kingdom). All of the other reagents, if not specified, were purchased from Sigma. The stable Hyp-DCHA (23) was prepared according to the method described in patent PCT WO 99/41220.

Cells

HT-1080 human fibrosarcoma, SK-N-BE human neuroblastoma, B16-LU8 mouse melanoma (kindly provided by Vincenzo Bronte, Department of Oncology, Medical School of Padova), and C-26 mouse colon adenocarcinoma cells were routinely grown in DMEM supplemented with 10% heat-inactivated FCS (Biochrom, Berlin, Germany). The medium was supplemented with 100 units/mL penicillin, 100 μg/mL streptomycin (and 20 μmol/L β-mercaptoethanol for B16-LU8), and the cells were incubated in 5% CO_2 in air at 37°C. Human umbilical vein endothelial cells (HUVECs) were isolated and grown following standard methods (26) . The C1-clone cells of the transgenic adenocarcinoma of mouse prostate (TRAMP-C1; ref. 27) were routinely grown in DMEM high glucose, with L-glutamine, and without sodium pyruvate media, supplemented with 5% nu-serum (Becton Dickinson Biosciences, St. Louis, MO), 5% heat-inactivated FCS, 5 μg/mL insulin, 25 units/mL penicillin-streptomycin, and 10^{-8} mol/L dihydrotestosterone.

Cell Growth Detection

HT-1080, SK-N-BE, B16-LU8, C-26, and TRAMP-C1 cells were plated onto 96-well plates at 10^4/well in culture medium with 10% heat-inactivated FCS and used after 24 hours. A 1 mmol/L stock solution of Hyp-DCHA was freshly prepared in methanol and added to cultures at final concentrations of 1, 3, 9, and 27 μmol/L. After 16 hours, the number of viable cells was determined by CellTiter 96 assay (Promega, Madison, WI) and expressed as ratio of absorbance ($A_{490\ nm}$) of treated *versus* control cells. HUVECs and HT-1080 cells were plated onto 96-well plates at 10^4/well in culture medium with heat-inactivated FCS and used after 24 h. Cells were treated with 9 μmol/L Hyp-DCHA, and their number of viable cells was determined as above after 7, 24, and 31 hours.

Long-Term Clonogenicity

Cell survival was tested by a clonogenic assay, as described previously (28) . HT-1080, treated 16 hours with 3, 9, and 27 μmol/L Hyp-DCHA as described above, were trypsinized, suspended in Hyp-DCHA-free medium, and tested for viability (parallel controls); 50 to 100 cells (depending on the survival percentage) were then reseeded in sextuplicates into 3.5-cm diameter plastic wells precoated overnight with FCS. After 1 week of incubation, colonies were fixed, stained with crystal violet, and counted. Plating efficiency of nontreated cells was taken as 100% survival.

Analysis of Total and Phosphorylated Extracellular Signal-Regulated Kinase 1/2 (ERK1/2)

C-26 colon carcinoma cells (5×10^5 for each sample) were suspended and rapidly lysed in 62 mmol/L Tris/HCl buffer (pH 6.8), containing 5% glycerol, 5% SDS, 0.5% β-mercaptoethanol, and protease inhibitor mixture (Calbiochem, Darmstadt, Germany). Cellular lysates were then subjected to SDS-PAGE (12% gels), transferred to nitrocellulose membranes, and immunostained with phospho-ERK1/2 antibody (Cell Signaling Technology, Beverly, MA) using an enhanced chemiluminescent detection system (Amersham Pharmacia Biotech, San Francisco, CA). Blots were then stripped and reprobed with ERK1/2 antibody (Cell Signaling Technology).

Cell Death Detection

HT-1080 cells were seeded (5×10^4) on glass coverslips and incubated at 37°C in 5% CO_2; after 24 h, the culture medium was replaced with fresh medium containing 9 μmol/L Hyp-DCHA, and after 7 and 24

hours, the cells were fixed with 4% paraformaldehyde for 30 minutes. In Situ Cell Death Detection kit, Fluorescein (terminal deoxynucleotidyl transferase-mediated nick end labeling; Roche, Mannheim, Germany), was used to measure apoptosis, and the cell nuclei were stained with Hoechst 33258; the samples were then analyzed by fluorescence microscopy.

Substrate Degradation by Serine-Proteinases

LE, cathepsin G, and thrombin were solubilized (250 mU/mL) in HEPES buffer (0.1 mol/L HEPES, 0.5 mol/L NaCl, 10% DMSO), pH 8.0 (elastase and thrombin), or pH 7.5 (cathepsin G); uPA (200 mU/mL) in 50 mmol/L Tris-HCl, 100 mmol/L NaCl (pH 7.4). The reagents were freshly solubilized (10 mmol/L) as follows: Hyp-DCHA in 100% methanol, elastase substrate in 100% ethanol, cathepsin G substrate in 100% DMSO, thrombin, and uPA substrates in H_2O. Dilutions of the inhibitor were premixed with the enzymes in plastic microwells (90 μl final volume), and after 15 minutes at 4°C, 10 μl of the appropriate substrate was added. The intensity of the color emitted by the digested substrates was monitored at 405 nm and the control background subtracted.

Modified Boyden Chamber Assay

The invasive behavior of HT-1080 and C-26 cells was tested using the modified Boyden chamber assay. Matrigel (Becton Dickinson, San Jose, CA) and gelatin were used as matrix for cells to migrate through toward a chemoattractant represented by serum-free culture medium conditioned 24 hours by NIH-3T3 fibroblasts (control experiments were performed in absence of chemoattractant). Polyvinylpyrrolidone-free polycarbonate filters (8-μm pore size) were all precoated by immersion in gelatin solution (0.1%) and part overcoated with 50 μL of 0.66 mg/mL Matrigel. After seeding of 8×10^4 cells onto the filters and 6 hours of incubation in serum-free medium with and without Hyp-DCHA, 0.1 and 0.5 μmol/L, nonmigrated cells were removed from the upper surface of the filter; this was rinsed in water and fixed with 100% ethanol for 30 seconds, then stained with toluidine blue for 10 minutes. The cells that actively migrated to the bottom surface of the filter were dissolved with 10% acetic acid and indirectly quantitated by measuring the absorbance at 590 nm. The results of sextuplicate experiments were averaged after background subtraction.

Zymographic Analysis

Aliquots of culture medium conditioned by HT-1080, B16-LU8, and C-26 cells incubated 6 hours in the presence of 0.1 to 1.0 μmol/L Hyp-DCHA were analyzed by gelatin zymography, as described previously (29) . Without heating and under nonreducing conditions, samples underwent electrophoresis in 0.1% gelatin-containing 8% polyacrylamide gels in presence of SDS. After electrophoresis, the gels were washed twice for 15 minutes with 2.5% Triton X-100, incubated overnight at 37°C in Tris buffer [50 mmol/L Tris-HCl, 200 mmol/L NaCl, and 10 mmol/L $CaCl_2$ (pH 7.4)], stained 30 minutes with 30% methanol/10% acetic acid containing 0.5% Coomassie Brilliant Blue R-250, and destained in the same solution without dye. The clear bands on the blue background, representing areas of gelatinolysis, were quantitated using an image analyzer system with GelDoc 2000 and Quantity One software (Bio-Rad, Hercules, CA).

For gelatinase inhibition assays, Hyp-DCHA was freshly solubilized in methanol and diluted (1, 10, and 100 μmol/L) in the Tris buffer used for developing separate slices of gelatinase zymograms, which were incubated as above.

Lung Colonization Model

Experiment A.

Thirteen male BALB/c mice of 17 to 19 g from Charles River (Lecco, Italy) were maintained 14 days in a germ-free environment and allowed free access to food and water before use. Then, 10 of them received an i.v. injection (tail vein) of C-26 single-cell suspension in sterile PBS (5×10^5 cells in 50-μL volume, 97% viability; ref. 30). Starting 7 days before inoculation of tumor cells, five animals received twice daily 150 μL of i.p. injections of 1 mmol/L Hyp-DCHA in 0.4% Tween 80, 10% DMSO (25) , and five animals received injections of vehicle only; three untreated mice were used as control. After 15 days, the mice were weighed, anesthetized, heparinized, and exsanguinated via the femoral artery; the heart and lungs were removed *en bloc*, the lungs were dissected away from the external vasculature and bronchi, weighed,

sectioned parasaggitally superior to inferior, and the specimens were fixed in buffered 4% paraformaldehyde for morphological studies.

Experiment B.

The experiment was repeated a second time with half number of C-26 cells, both with and without 7-day Hyp-DCHA pretreatment; in the second case, the treatment was initiated at the time of cell injection. The animals were sacrificed after 17 days.

Experiment C.

The same pretreatment protocol was used also for mice (syngeneic C57BL/6, six/group) injected i.v. with 10^5 B16-LU8 cells, the treatment continued as above, and the experiment concluded after 18 days.

Measurement of Hyp Blood Level

For determination of Hyp level, blood samples were obtained from BALB/c mice 30 minutes after injection of Hyp-DCHA as above (hematic peak; ref. 25), and the plasma was mixed with 2 volumes of ethanol and centrifuged; the supernatant was then vacuum-dried and solubilized in methanol. Hyp was identified and quantified by high-performance liquid chromatography, using a Chromquest P4000 pump (Thermoseparation, San Jose, CA) equipped with a photodiode array detector (UV6000), and a RP-18 column Vydac (5 μm) eluted with a water-methanol-acetonitrile-phosphoric acid mobile-phase system, according to Brolis *et al.* (31) . The limit of quantification was determined by the lowest Hyp concentration of the standard curve and corresponded to 0.6 μg/mL (1.2 μmol/L; $r^2 = 0.9999$).

Pathology

Experiment A and B.

Before sectioning, all lungs were photographed to document size and subpleural metastatic involvement. Specimens from different lobes embedded in paraffin were serially sectioned at 5 μm and stained in H&E. The surface area of all metastatic nodules present in the serial sections of both lungs of each animal were measured using computerized morphometry with an image analyzer system (TV camera 3CCD JVC; Olympus microscope; personal computer with Image-Pro Plus software version 4.1; Media Cybernetics, Silver Spring, MD). The morphometric evaluation was performed on only 1 of 10 serial sections per lung lobe (5 in mouse), the most suitable one for morphometric analysis in terms of sharpness, staining, minimal procedural artifacts, and so forth. The total analyzed lung parenchyma area ranged from 14 to 16 mm^2 in the smaller lungs and from 45 to 52 mm^2 in the larger. The values were expressed as a percentage of total analyzed area. Slides from the two groups of mice were randomized, coded, and examined blind without knowledge of the treatment.

Experiment C.

For this experiment, where the metastatic subpleural black nodules were clearly evident, the number of metastases on both lungs was macroscopically counted (without sectioning) ranking the nodules as small (<0.5 mm) and medium-large (>0.5 mm).

Statistical Analysis

The data from *in vitro* experiments were analyzed for significance using Student's t test (two tailed); those from *in vivo* experiments were analyzed using ANOVA and Student's *t* test for differences between subgroups. Differences were considered statistically significant at a level of $P < 0.05$.

RESULTS

Hyp-DCHA Inhibits Tumor Cell Growth and Survival *In vitro*.

The potential of Hyp-DCHA to inhibit cell growth was evaluated in human (HT-1080 and SK-N-BE) and murine (B16-LU8, C-26, and TRAMP-C1) cancer cell lines by cell viability kit. Growth of all cell lines was inhibited to varying degrees by Hyp-DCHA: B16-LU8, HT-1080, and C-26 were the more sensitive, with

IC_{50} = 5 to 8 μmol/L (Fig. 2*A*) ⇓ . Incubation of cells in solvent-containing medium (1% methanol) did not affect cell growth (data not shown). The inhibitory effect of Hyp-DCHA on cell growth was further studied in human HT-1080 and HUVECs, and exposed for different times (7, 24, and 31 hours) to 9 μmol/L Hyp-DCHA; as shown in Fig. 2*B* ⇓ , whereas in both cell lines, the growth was slightly restrained after 7 hours, the growth fell 23 ± 4.5% for HUVECs and 70 ± 3.5% for HT-1080 after 31 hours. One-week clonogenic assay of 16-hour-treated cells confirmed a Hyp-DCHA-triggered dose-response effect, with 71 ± 11, 36 ± 9, and 19 ± 6% survival at 3, 9, and 27 μmol/L Hyp-DCHA, respectively, on HT-1080, and a lower effect on HUVECs (56 ± 8% at 27 μmol/L Hyp-DCHA).

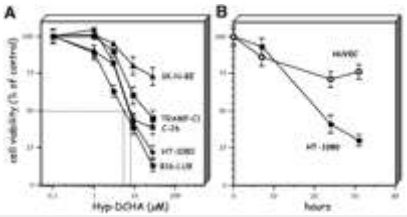

Fig. 2.

Effect of increasing concentrations of Hyp-DCHA on the growth of different cell lines. *A*. Human HT-1080 and SK-N-BE and murine B16-LU8, C-26, and TRAMP-C1 cells were grown in 96-well plates to a density of 10^4/well and then incubated in the presence of Hyp-DCHA (1, 3, 9, and 27 μmol/L) for 16 hours. The number of viable B16-LU8 and HT-1080 cells was reduced the most, followed by C-26. *B*. HT-1080 cells and HUVECs were seeded as above and treated with Hyp-DCHA (9 μmol/L); the number of viable cells was assayed after 7, 24, and 31 hours, and the percentage of viable cell calculated as ratio of the absorbance ($A_{490\ nm}$) of treated *versus* control cells. Examples of triplicate experiment; average of sextuplicates ± SD.

Hyp-DCHA-Induced Apoptotic Cell Death in HT-1080.

As previously reported (7) , inhibition of tumor cells growth by Hyp-DCHA was associated with induction of apoptosis (Fig. 3) ⇓ . In addition, compared with control cells (Fig. 3*A*) ⇓ , we now report that HT-1080 cells treated for 7 hours with 9 μmol/L Hyp-DCHA show typical alterations of membrane morphology (membrane blebs), which are associated with early apoptosis (arrows in Fig. 3*B* ⇓). In HT-1080 cells treated with the Hyp-DCHA for 24 hours (phase contrast in Fig. 3*D* ⇓ *versus* control Fig. 3*C* ⇓), chromatin condensation was revealed by Hoechst staining (arrows in Fig. 3*F* ⇓ ; negative control in Fig. 3*E* ⇓), and late apoptosis (DNA fragmentation) detected by terminal deoxynucleotidyl transferase-mediated nick end labeling assay (arrows indicate positive nuclei in Fig. 3*H* ⇓ ; negative control in Fig. 3*G* ⇓).

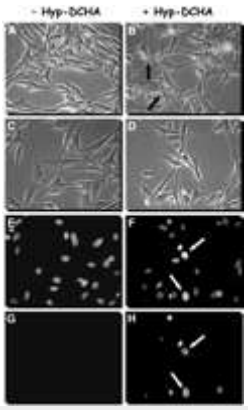

Fig. 3.

Induction of apoptosis by 9 μmol/L Hyp-DCHA in HT-1080 cells. *A* and *B*, phase contrast photomicrographs of HT-1080 cells incubated 7 hours ±9 μmol/L Hyp-DCHA; the *arrows* indicate cellular membrane alterations (blebs). *C* and *D*, cells incubated 24 hours as above. *E* and *F*, Hoechst staining of the cells in *C* and *D*, with *arrows* indicating chromatin condensation. *G* and *H*, terminal deoxynucleotidyl transferase-mediated nick end labeling of the cells in *C* and *D*, with *arrows* indicating DNA fragmentation.

Effect of Hyp-DCHA on Protease Activity.

To assay the inhibition exerted by Hyp-DCHA on human serine-proteases, purified enzymes—LE, thrombin, cathepsin G, and uPA—were incubated with their respective synthetic substrate and the digestion colorimetrically monitored.

The activity of LE (5 mU on 500 μmol/L substrate) was strongly inhibited by Hyp-DCHA, with IC_{50} = 3 μmol/L (Fig. 4) ⇓ ; the inhibition exerted was dose dependent and noncompetitive, as determined by double-reciprocal plotting of the results obtained at different Hyp-DCHA concentrations, and the calculated Ki was 4.9 μmol/L (data not shown). The deduced IC_{50} values for cathepsin G, thrombin, and uPA (5 mU on 100 μmol/L-, 50 mU on 500 μmol/L-, and 20 mU on 500 μmol/L-specific substrates) were 20, 40, and 40 μmol/L, respectively (Fig. 4) ⇓ .

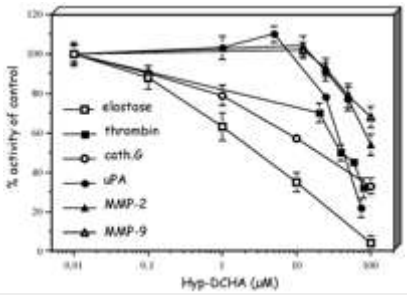

Fig. 4.

Dose-response inhibition of proteolytic activities by Hyp-DCHA. LE, cathepsin-G, thrombin, and uPA activity were measured against specific chromogenic substrates, and MMP-2 and MMP-9 activity were measured by gelatin zymography. Examples of triplicate experiment; average of sextuplicates ± SD.

Lower inhibition was registered on the MMPs 2 and 9 when gelatin zymography assay was developed in the presence of Hyp-DCHA; no effect was registered up to 10 μmol/L and the $IC_{50} \geq 100$ μmol/L (Fig. 4) ⇓ .

Effect of Hyp-DCHA on Matrigel Invasion.

The modified Boyden chamber assay showed that Hyp-DCHA exerts a dose-dependent inhibition of human HT-1080 cells chemoinvasion through Matrigel (reconstituted basement membrane), with an IC_{50} in the range of 0.1 μmol/L (Fig. 5*A*) ⇓ ; compared with the control, the number of cells recovered on the bottom side of the Matrigel-coated filters was reduced by 46 ± 8% ($P = 0.007$) and 62 ± 7% ($P < 0.0005$) with 0.1 and 0.5 μmol/L Hyp-DCHA, respectively. In contrast, migration to a chemoattractant (chemotaxis) through gelatin-coated filters remained unaffected (Fig. 5*B*) ⇓ . The restraint of chemoinvasion was less pronounced in TRAMP-C1 cells and <30% at 0.5 μmol/L Hyp-DCHA (data not shown). Control experiments contained 1% methanol, the solvent used to solubilize Hyp-DCHA.

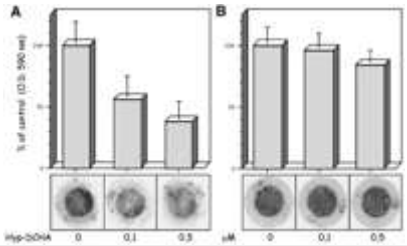

Fig. 5.

Effects of Hyp-DCHA on HT-1080 cells chemoinvasion and chemotaxis. *A*. HT-1080 cells were seeded onto Matrigel (*A*)- or gelatin (*B*)-coated filters, mounted on Boyden chambers, and exposed for 6 hours to a chemoattractant. The number of cells on the bottom side of the filters (examples boxed at the bottom of the histograms) was then quantitated and expressed in the histogram as percentage of controls. In the presence of Hyp-DCHA, the chemoinvasion (*A*), but not the chemotaxis (*B*), was restrained, with $P = 0.007$

(0 *versus* 0.1 μmol/L), and $P < 0.0005$ (0 *versus* 0.5 μmol/L). Examples of triplicate experiment; average of sextuplicates + SD.

Hyp-DCHA Effects on Invasion and Gelatinase Expression.

The potential influence of Hyp-DCHA on chemoinvasion through Matrigel was also examined in mouse C-26 cells. In the presence of 0.1 and 0.5 μmol/L Hyp-DCHA (below the cytotoxicity threshold), cell invasiveness was inhibited by 20 ± 5% ($P = 0.0015$) and 80 ± 4% ($P < 0.0001$), respectively (Fig. 6*A*) ⇓ , as compared with control cells incubated with solvent-containing medium. Gelatin zymography of 45 μL of medium conditioned 6 hours by C-26 cells, mixed with 15 μL of 4× sample buffer, revealed the presence of two major gelatinolytic activities corresponding to MMP-2 and MMP-9 (as determined by comparison with mouse-serum control enzymes; data not shown). Zymography of an equal volume of medium conditioned by the same number of cells incubated 6 hours in the presence of 0.5 μmol/L Hyp-DCHA revealed gelatinolytic bands of clearly lower intensity (Fig. 6*B*) ⇓ . This was not the case when the medium conditioned by control cells (0 μmol/L Hyp-DCHA) was preincubated 6 hours in a test tube with the same concentration of Hyp-DCHA (Fig. 6*C*) ⇓ .

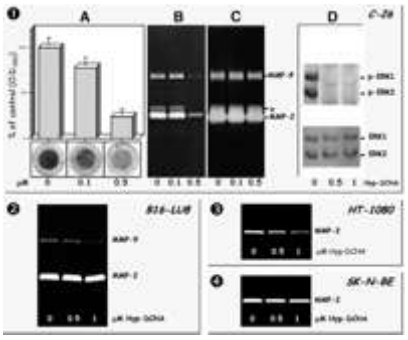

View larger version:

In this page
In a new window

Download as PowerPoint Slide

Fig. 6.

Effect of Hyp-DCHA on chemoinvasion, gelatinase expression, and kinase activity. *First panel: A*. C-26 cell chemoinvasion through Matrigel, assayed as in Fig. 5 ⇓ *A*, was significantly inhibited even by 0.1 μmol/L Hyp-DCHA: $P = 0.0015$ (0 *versus* 0.1 μmol/L) and $P < 0.0001$ (0 *versus* 0.5 μmol/L). Examples of triplicate experiment; average of sextuplicates + SD (example filters boxed at the bottom of the histograms). *B*, gelatin zymography of equal volumes of medium conditioned by C-26 cells incubated 6 hours in the presence of 0, 0.1, and 0.5 μmol/L Hyp-DCHA shows that the latter concentration triggers a strong decrease of pro-MMP-2 and pro-MMP-9 activities. This is not due to an electrophoresis-resistant inhibitor/enzyme binding, as verified in *C* when the clarified control medium (0 μmol/L Hyp-DCHA) from the experiment in *B* was incubated with the indicated concentrations of Hyp-DCHA before electrophoresis, and no reduction of gelatinolytic activity was revealed by the zymographic assay. ∗ = unidentified. *D*, comparable aliquots of lysate of C-26 cells, cultured in the absence or presence of Hyp-DCHA for 3 hours, were analyzed sequentially using antibodies against diphosphorylated (active) *p*-ERK1/2 (*top inset*) and nonphosphorylated ERK1/2 (*bottom inset*). Figure representative of two separate experiments. *Second through fourth panels:* gelatin zymography shows that 1 μmol/L Hyp-DCHA down-modulates MMP-9 activity in B16-LU8, and MMP-2 in HT-1080, but not in SK-N-BE cells.

In the presence of Hyp-DCHA, the gelatinase expression by other cell lines was restrained to a lower extent (Fig. 6) ⇓ ; at 1 μmol/L, only MMP-9 was down-modulated in B16-LU8, and MMP-2 was restrained in HT-1080 but not in SK-N-BE cells (in both, MMP-9 not expressed).

Hyp-DCHA Effects on ERK1/2.

Because the activation of the raf/MEK/ERK signaling pathway has been reported to induce the enhancement of MMP expression (32, 33, 34) , the potential influence of Hyp-DCHA on the activity of ERK1/2 was tested. To this purpose, protein lysates of control and treated C-26 cells were subjected to Western blot analysis for phosphorylated (active) as well as total ERK1/2 protein kinases. Although in control conditions ERK1/2 are constitutively highly phosphorylated in these malignant cells, 3 hours of incubation with 0.5 μmol/L Hyp-DCHA abolished both protein kinase activation, as judged from the lack of immunostaining with specific antibody (Fig. 6*D*) ⇓ . Inhibitory effect on ERK1/2 kinases was also found in B16-LU8 cells treated with Hyp-DCHA (data not shown).

Lung Colonization under Hyp-DCHA.

Intraperitoneal administration of Hyp-DCHA, 1 mmol/L in 150 μL, twice daily for 22 days, starting 7 days before syngeneic C-26 or B16-LU8 tumor i.v. inoculation, registered some nonmarginal effects even before animal sacrifice; treated mice (+tm) appeared healthy during the experiment, whereas the vehicle-administered ones (−tm) became moribund and presented signs of dyspnea, ataxia, and characteristic fur changes the second week after tumor inoculation. The same effect was registered without 7-day pretreatment.

The level of Hyp in the blood of BALB/c-treated mice was measured at 30 minutes after i.p. injection, when the hematic peak is reached (25) , and was always lower than the *in vitro* cytotoxic threshold for the injected cells (C-26), with concentrations <1.2 μmol/L (data not shown). At the end of experiment A, the average weight of +tm was equivalent to that of normal animals (22.6 ± 1.0 *versus* 23.2 ± 1.0 g, respectively; $P = 0.343$), whereas that of −tm was significantly lower (17.4 ± 0.6 g, $P = 0.007$). Autopsy showed that although the mean lung weight of +tm was moderately but not significantly higher than that of normal animals (0.48 ± 0.148 and 0.31 ± 0.014 g, respectively; $P = 0.056$), that of −tm was almost three times higher (0.92 ± 0.051 g; $P < 10^{-7}$), and the difference between treated and untreated tumor-bearing mice was highly significant ($P < 0.001$; Fig. 7*A* ⇓).

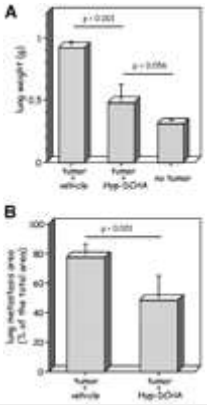

Fig. 7.

The effect of Hyp-DCHA treatment on experimental lung metastases. Intraperitoneal administration of Hyp-DCHA, 1 mmol/L in 150 μL, twice daily for 22 days, starting 7 days before syngeneic C-26 tumor i.v. inoculation into BALB/c mice, resulted in a strong decrease in lung weight, and metastasis extension. *A*. The mean lung weight of Hyp-DCHA mice was just above that of non-tumor-bearing animals (0.48 *versus* 0.31 g); in contrast, the mean lung weight in vehicle-administered animals was twice as high (0.92 g). *B*. The mean area of lung metastases of Hyp-DCHA mice was 48.3% of the lung section area, whereas that of vehicle-administered animals was 77.4%. The number of mice per group was: five (tumor + vehicle), five (tumor + Hyp-DCHA), and three (no tumor).

In experiments A and B (with C-26 cells), the subpleural surface of −tm mice was comprised of metastatic nodules macroscopically larger that those present in +tm with pretreatment (Fig. 8, *A* ⇓ *versus D*). Morphometric analysis of neoplastic areas, equally distributed in both lungs, revealed a mean area significantly lower, −38%, in +tm with pretreatment in comparison to −tm (48.3 ± 5.1 *versus* 77.4 ± 9.3

percentage of total section, respectively, $P < 0.001$; Figs. 7*B* ⇓ and 8 ⇓). When the experiment was repeated injecting a lower number of tumor cells, the reduction was −36% (51.8 ± 6.9 *versus* 70.0 ± 8.5, $P < 0.02$), and equivalent reduction, −33%, was registered in animals without Hyp-DCHA pretreatment (55.4 ± 5.9 *versus* 72.1 ± 8.0, $P < 0.02$); the difference between groups with and without pretreatment was not significant.

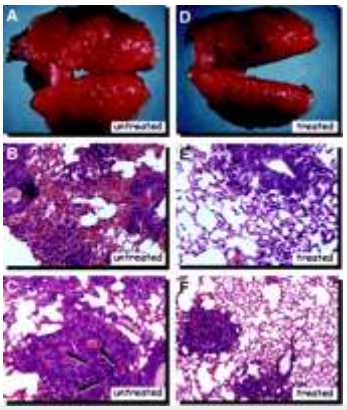

Fig. 8.

The effect of Hyp-DCHA treatment on experimental lung metastases (sample photographs from mice as in Fig. 7 ⇓). *A* and *D*, macroscopic view of lungs: more numerous and larger subpleural metastatic bulges are visible in the untreated *versus* the treated animal. *B* and *E*, histological section of lung metastatic foci: note a massive congestion, edema, and inflammation in the untreated animal and the mild inflammatory cell infiltration in the treated mice (H&E, ×25). *C* and *F*, large metastatic nodules showing much more diffuse neovascularization (*arrows*) in the untreated *versus* the treated animal (H&E, ×25).

Blood vessels of various sizes were always present within the majority of large metastatic nodules in the lungs of −tm, whereas only rarely in those of +tm (Fig. 8, *C* ⇓ *versus F*). In the first case, more frequent and heavier inflammatory cell congestion and edema were observed, sometimes with the presence of necrotic foci (Fig. 8, *B* ⇓ *versus E*). In this very crowded, but nonetheless self-evident, histopathological picture, individual morphometric analysis of these parameters was not performed; these were in line with previously reported results (30 , 35) .

Reduction of metastatic aggressiveness was also registered using a different experimental metastasis model, B16-LU8 in C57BL/6 mice, and counting the subpleural black nodules. Under Hyp-DCHA regimen, the mean number of lung metastases was <22% (79.4 ± 9 *versus* 101.8 ± 12, $P = 0.01$), with reduction of mainly medium-large size nodules, >0.5 mm).

DISCUSSION

In the present article, noncytotoxic Hyp-DCHA concentrations are shown to restrain some proteolytic activities instrumental to matrix degradation and to inhibit invasion and metastasis in murine colon carcinoma and melanoma models.

Hyp-DCHA inhibits to varying degrees tumor cell growth, with IC_{50} in the range of 5 to 20 μmol/L for the highly invasive B16-LU8, HT-1080, C-26, and TRAMP-C1 cell lines and with lower efficacy for the SK-N-BE line, but these concentrations have much lower effect on nontransformed endothelial cells (HUVECs), as confirmed by clonogenic assay. Similar differential susceptibility has already been reported for other plant compounds, notably for (-)epigallocatechin-3-gallate (18) , which inhibits cyclin-dependent kinases (36) . Differences in proliferation rates may indeed account for the differential restraint under Hyp-DCHA, and it seems reasonable to expect that *in vivo* not all types of tumor respond equally to this drug. Considering also that treatment of tumor cells with Hyp-DCHA resulted in apoptosis-specific morphological changes (such as flare-up of apoptotic oligonucleosomes) at concentrations not effective in HUVECs, these

observations strengthen the possibility of preferentially targeting the Hyp-DCHA-triggered cytotoxic effect to tumor cells.

On account of this property, Hyp has already been proposed as a new cytotoxic drug against cancer (5) . The stronger anti-invasive property, now reported for Hyp-DCHA, reinforces this proposal. Concentrations of Hyp-DCHA ≥ 20-fold below the toxicity threshold on HT-1080 and C-26 tumor cells were very effective in inhibiting the *in vitro* invasive behavior in these cells, but less in TRAMP-C1 cells, despite all three types being highly metastatic. Invasiveness inhibitors may act by down-modulating extracellular-barrier degrading proteinases such as MMP-2 and MMP-9 (37 , 38) and LE (20) , which, in addition, can activate a number of MMPs (39) . Here, zymographic assays showed full development of the gelatinolytic potential of MMP-2 and MMP-9 also in the presence of invasion-restraining concentration of Hyp-DCHA (IC_{50} < 0.5 μmol/L); this indicates that the effect registered *in vitro* cannot be triggered by a direct inhibition of their activity, which is in fact hindered at concentrations 200-fold higher (IC_{50} > 100 μmol/L; Fig. 4 ⇓).

On the other hand, what did register a remarkable reduction was the gelatinolytic activity of both MMP-2 and MMP-9 in the media conditioned by C-26 cells (and to a lower extent by other metastatic cell lines) incubated in the presence of μmol/L Hyp-DCHA (Fig. 6*B*) ⇓ . This reduction was shown not to be attributable to an electrophoresis-resistant MMP-Hyp binding, which could inhibit the gelatinolytic activity during the zymographic development. Although the lack of cytoskeleton impairment, evidenced by chemotaxis experiments, reveals no effect on cell motility, it seems reasonable to assume that the inhibition of C-26 and HT-1080 invasion, triggered *in vitro* by Hyp-DCHA, is the result of a substantial down-regulation of the release and/or synthesis of the two MMPs. Assuming that other proteinases trigger invasion in TRAMP-C1, the much lower secretion of MMP-2 by these cells (data not shown) in comparison to C-26 and HT-1080 also supports the above assumption.

Metalloproteinase synthesis and function are regulated at multiple levels, including transcriptional activation. In particular, up-regulation of MMP expression has been reported to be dependent on activation of the raf/MEK/ERK signaling pathway, which strictly regulates gene expression (31, 32, 33) . Consistently, whereas the high expression of MMP-2 and MMP-9 in C-26 cells correlates with constitutive activation of ERK1/2 protein kinases (Fig. 6*D*) ⇓ , treatment of these cells with Hyp-DCHA inhibits both ERK1/2 kinase activity and MMP-2 and MMP-9 expression (Fig. 6*B*) ⇓ . This restraint of the metastatic aggressiveness is thus, at least for this aspect, triggered by the hindering of this signal transduction pathway (33) .

Moreover, it is worth noting that the activity of other matrix proteinases is directly restrained at concentrations much lower than those inhibiting MMP-2 and MMP-9. The two enzymes most sensitive to Hyp-DCHA, LE, and cathepsin G (IC_{50} = 3 and 20 μmol/L, respectively) are expressed by inflammatory cells, in particular the polymorpho-nuclear phagocytes. These cells, by triggering oxidative stress, angiogenesis, and matrix degradation, may represent a serious promoting or aggravating event for tumor onset, growth, and spread (41) . Because Hyp can interact with COX-1 and 5-LO (42) , the inhibition of proinflammatory eicosanoid production from arachidonic acid may *in vivo* synergize with inhibition of LE activity and contribute to the eventual restraint of metastatic spreading registered *in vivo* (see below).

The restraint of gelatinase expression and the *in vitro* anti-invasive effect (in absence of polymorpho-nuclear phagocytes) exerted by Hyp-DCHA were triggered at concentrations of Hyp detected in the blood of patients (0.3 to 0.45 μmol/L) after administration of mood-lifting therapeutic doses of St. John's wort extracts (3 × 300 mg daily; ref. 22). This observation substantiates the clinical relevance of our findings and prompts a study of the cancer epidemiology of patients following this antidepressant treatment. Meanwhile, the results from the experimental metastasis model in mice who received i.v. injections of syngeneic colon carcinoma (C-26) or melanoma (B16-LU8) cells and twice daily i.p. with Hyp-DCHA are very encouraging: first of all, the Hyp-DCHA treatment resulted in preservation of normal body-weight gain, a more active behavior, and much lower impairment, as registered at the end of the experiment; in contrast, untreated tumor-bearing animals reached only 75% of control body weight and presented signs of dyspnea and ataxia.

Moreover, the Hyp-DCHA regimen resulted in a dramatic reduction of lung weight, −48%, C-26 in BALB/c, and in a significant containment of both pulmonary parenchyma occupied by metastases, −38%, and number of subpleural metastatic nodules, −22%, in the colon carcinoma C-26 and melanoma B16-LU8, respectively. Although in the animals without Hyp-DCHA pretreatment the restraint of overall metastatic aggressiveness was equivalent, the treatment protocols deserve to be studied in more detail to enable the potential benefits to be maximized. Whether and to what extent the inhibition of growth already reported for Hyp topically injected into primary tumors (6) is exerted also on the growth of metastatic foci by Hyp-DCHA injected i.p., as it could be inferred from the greater reduction of metastatic burden *versus* number of foci, remains to be verified in each model system.

Although the restraint of number and growth of metastases cannot be attributable to direct cell killing by Hyp (its blood level was always lower than the cytotoxic threshold), the effect on lung weight must be considered only a partial indicator of metastatic involvement. In fact, the lung parenchyma of untreated mice showed massive inflammatory cell infiltration, severe congestion, and edema, which add considerably to the registered weight, and in the untreated animals, the tissue was nourished by a much-developed vascular network of neoformation (Fig. 8) ⇓ , as reported previously (30) .

Overall, these results show that Hyp has the potential of reducing invasion and metastasis in parallel with a remarkable restraint of the raf/MEK/ERK signaling pathway that leads to down-regulation of MMP-2 and MMP-9 expression by tumor cells, as mostly registered in the C-26 model; then, the restraint of inflammatory recruitment (Refs. 35 , 41 , 42 and here), LE activity, and tumor neovascularization (Ref. 30 and here) may contribute to the containment of subsequent growth of the metastatic foci. These suggestions are consistent with the control, in the same murine C-26 model, of both angiogenesis and metastasis by a synthetic MMP inhibitor (29) . Whether and to what extent these effects are a general outcome of Hyp regimen remains to be investigated on different types of tumor.

Our results were obtained using an experimental metastasis model (i.v. injection). However, an even more pronounced protective effect should be registered in spontaneous metastasis models where more steps of the process can be hindered by Hyp, including cell proliferation and survival, as already proved (ref. 6 and here), as well as intravasation.

In humans, it has been reported that Hyp can alter the pharmacokinetics of many important pharmaceuticals (43) , including anticancer drugs (44) , potentially mitigating their effects (1) . Even so, Hyp could prove itself as a new drug for anticancer treatment, replacing others currently in use. On the other hand, Hyp has been shown to be amenable to chemical modification (24) , and the inhibition of metastatic aggressiveness and the induction of P450 (detoxifying system) could be appropriately dissected.

Acknowledgments

We thank Professor Michele Spina (Department Experimental Biomedical Sciences, Medical School of Padova) for helpful discussion in the preparation of the revised form and Dr. Susan Biggin for editorial revision and valuable suggestions.

Footnotes

Grant support: Associazione Italiana per la Ricerca sul Cancro, Ministero dell'Istruzione Universitá e Ricerca Italian Government (project "Sostanze Naturali ed Analoghi Sintetici con Attività Antitumorale"), and University of Padova (Padova, Italy).

The costs of publication of this article were defrayed in part by the payment of page charges. This article must therefore be hereby marked *advertisement* in accordance with 18 U.S.C. Section 1734 solely to indicate this fact.

Note: M. Donà and I. Dell'Aica contributed equally to the present work.

Requests for reprints: Spiridione Garbisa, Department of Experimental Biomedical Sciences, viale G. Colombo 3, 35121 Padova, Italy. Phone: 0039-049-8276088; Fax: 0039-049-8276089; E-mail garbisa@unipd.it.

↵6 Internet address: http://nccam.nih.gov/news/2003/032103.htm.

Received January 28, 2004.
Revision received June 14, 2004.
Accepted July 2, 2004.

References

1. ↵
Barnes J, Anderson LA, Phillipson JD St. John's wort (Hypericum perforatum L.): a review of its chemistry, pharmacology and clinical properties. J Pharm Pharmacol, 53: 583-600, 2001.
2. ↵
Mansky PJ, Straus SE St. John's wort: more implications for cancer patients. J Natl Cancer Inst (Bethesda), 94: 1157-8, 2002.
3. ↵
Watkins RE, Maglich JM, Moore LB, et al 2.1 Å crystal structure of human PXR in complex with the St. John's wort compound hyperforin. Biochemistry, 42: 1430-8, 2003.
4. ↵
Schempp CM, Pelz K, Wittmer A, Schöpf E, Simon JC Antibacterial activity of hyperforin from Saint John's wort, against multiresistant Staphylococcus aureus and Gram-positive bacteria. Lancet, 353: 2129 1999.
5. ↵
Schempp CM, Winghofer B, Ludtke R, Simon-Haarhaus B, Schöpf E, Simon JC Topical application of St. John's wort (Hypericum perforatum L.) and of its metabolite hyperforin inhibits the allostimulatory capacity of epidermal cells. Br J Dermatol, 142: 979-84, 2000.
6. ↵
Schempp CM, Kirkin V, Simon-Haarhaus B, et al Inhibition of tumor cell growth by hyperforin, a novel anticancer drug from St. John's wort that acts by induction of apoptosis. Oncogene, 21: 1242-50, 2002.
7. ↵
Hostanska K, Reichling J, Bommer S, Weber M, Saller R Hyperforin a constituent of St. John's wort (Hypericum perforatum L.) extract induces apoptosis by triggering activation of caspases and with hypericin synergistically exerts cytotoxicity towards human malignant cell lines. Eur J Pharm Biopharm, 56: 121-32, 2003.
8. ↵
Liotta LA, Tryggvason K, Garbisa S, Hart I, Foltz CM, Shafie S Metastatic potential correlates with enzymatic degradation of basement membrane collagen. Nature (Lond.), 284: 67-8, 1980.
9. ↵
Watanabe H, Nakanishi I, Yamashita K, Hayakawa T, Okada Y Matrix metalloproteinase-9 (92 kDa gelatinase/type IV collagenase) from U937 monoblastoid cells: correlation with cellular invasion. J Cell Sci, 104: 991-9, 1993.
10. ↵
Azzam HS, Arand G, Lippman ME, Thompson EW Association of MMP-2 activation potential with metastatic progression in human breast cancer cell lines independent of MMP-2 production. J Natl Cancer Inst (Bethesda), 85: 1758-64, 1993.
11. ↵
Liotta LA, Steeg PS, Stetler-Stevenson WG Cancer metastasis and angiogenesis: an imbalance of positive and negative regulation. Cell, 64: 327-36, 1991.
12. ↵
Eccles SA, Box GM, Court WJ, Bone EA, Thomas W, Brown PD Control of lymphatic and hematogenous metastasis of a rat mammary carcinoma by the matrix metalloproteinase inhibitor batimastat (BB-94). Cancer Res, 56: 2815-22, 1996.
13. ↵
Coussens LM, Fingleton B, Matrisian LM Matrix metalloproteinase inhibitors and cancer: trials and tribulations. Science (Wash. DC), 295: 2387-92, 2002.

14. ↵
Wang ZY, Huang MT, Ho CT, et al Inhibitory effect of green tea on the growth of established skin papillomas in mice. Cancer Res, 52: 6657-65, 1992.
15. ↵
Cao Y, Cao R Angiogenesis inhibited by drinking tea. Nature (Lond.), 398: 381 1999.
16. ↵
Garbisa S, Biggin S, Cavallarin N, Sartor L, Benelli R, Albini A Tumor invasion: molecular shears inhibited by green tea. Nat Med, 5: 1216 1999.
17. ↵
Taniguchi S, Fujiki H, Kobayashi H, et al Effect of (-)-epigallocatechin gallate, the main constituent of green tea, on lung metastasis with mouse B16 melanoma cell lines. Cancer Lett, 65: 51-4, 1992.
18. ↵
Garbisa S, Sartor L, Biggin S, Salvato B, Benelli R, Albini A Tumor gelatinases and invasion inhibited by green tea flavanol (-)epigallocatechin-3-gallate. Cancer (Phila.), 91: 822-32, 2001.
19. ↵
Demeule M, Brossard M, Page M, Gingras D, Beliveau R Matrix metalloproteinase inhibition by green tea catechins. Biochim Biophys Acta, 1478: 51-60, 2000.
20. ↵
Sartor L, Pezzato E, Garbisa S (-)Epigallocatechin-3-gallate inhibits leukocyte elastase: phytofactor for hindering inflammation, emphysema and invasion. J Leuk Biol, 71: 73-9, 2002.
21. ↵
Lambert JD, Lee M-J, Lu H, et al Epigallocatechin-3-gallate is absorbed but extensively glucuronidated following oral administration to mice. J Nutr, 133: 4172-7, 2003.
22. ↵
Biber A, Fisher H, Romer A, Chatterjee SS Oral bioavailability of hyperforin from Hypericum extracts in rats and human volunteers. Pharmacopsychiatry, 31: 36-43, 1998.
23. ↵
Chatterjee SS, Erdelmeier C, Klessing K, Marmé D, Schächtele C. Stable hyperforin salts: method for producing them and their use in the treatment of Alzheimer's disease. PCT WO 99/41220, 1999 August 19.
24. ↵
Verotta L, Appendino G, Belloro E, et al Synthesis and biological evaluation of Hyperforin analogues. Part I. Modification of the enolized cyclohexanedione moiety. J Nat Prod, 65: 433-8, 2002.
25. ↵
Cervo L, Rozio M, Ekalle-Soppo CB, Guiso G, Morazzoni P, Caccia S Role of Hyperforin in the antidepressant-like activity of Hypericum perforatum extracts. Psychopharmacology, 164: 423-8, 2002.
26. ↵
Gimbrone MA, Jr, Shefton EJ, Cruise SA Isolation and primary culture of endothelial cells from human umbilical vessels. Tissue Culture Association Manual, 4: 813-8, 1978.
27. ↵
Foster BA, Gingrich JR, Kwon ED, Madias C, Greenberg NM Characterization of prostatic epithelial cell lines derived from transgenic adenocarcinoma of the mouse prostate (TRAMP) model. Cancer Res, 57: 3325-30, 1997.
28. ↵
Valduga G, Reddi E, Garbisa S, Jori G Photosensitization of cells with different metastatic potentials by liposome-delivered Zn-(II)-phthalocyanine. Int J Cancer, 75: 412-7, 1998.
29. ↵
Brown PD, Bloxidge RE, Anderson E, Howell A Expression of activated gelatinase in human invasive breast carcinoma. Clin Exp Metastasis, 11: 183-9, 1993.
30. ↵
Lozonschi L, Sunamura M, Kobari M, Egawa S, Ding L, Matsuno S Controlling tumor angiogenesis and metastasis of C26 murine colon adenocarcinoma by a new matrix metalloproteinase inhibitor, KB-R7785, in two tumor models. Cancer Res, 59: 1252-8, 1999.
31. ↵
Moon SK, Lee YC, Kim CH. Disialo ganglioside (GD3) synthase gene expression suppresses vascular smooth muscle cell responses via the inhibition of ERK1/2 phosphorylation, cell cycle progression, and matrix metalloproteinase-9 expression. J Biol Chem;2004 June 2 [epub ahead of print].
32. ↵
Westermarck J, Kähäri V-M Regulation of matrix metalloproteinase expression in tumor invasion. FASEB J, 13: 781-92, 1999.

33. ↵
Chung T-W, Lee Y-C, Kim C-H. Hepatitis B viral HBx induces matrix metalloproteinase-9 gene expression through activation of ERKs and PI-3K/AKT pathways: involvement of invasive potential. FASEB J 2004 May 7 [epub ahead of print].
34. ↵
Brolis M, Gabetta N, Fuzzati R, Pace R, Panzeri F, Peterlongo F Identification by high-performance liquid chromatography-diode array detection- mass spectrometry and quantification by high-performance liquid chromatography-UV absorbance detection of active constituents of Hypericum perforatum. J Chromatogr A, 825: 9-16, 1998.
35. ↵
Schempp CM, Simon JC. Use of hyperforin and derivatives thereof for inhibiting angiogenesis, and therapeutic use. PCT WO 03/EP4748, 2003 May 6.
36. ↵
Liang JC, Lin-Schiau SY, Chen CF, Lin JK Inhibition of cyclin-dependent kinases 2 and 4 activities as well as induction of CDK inhibitors p21 and p27 during growth arrest of human breast carcinoma cells by (-)epigallocatechin-3-gallate. J Cell Biochem, 75: 1-12, 1999.
37. ↵
Sugiura Y, Shimada H, Seeger RC, Laung WE, DeClerck YA Matrix metalloproteinases-2 and -9 are expressed in human neuroblastoma: contribution of stromal cells to their production and correlation with metastasis. Cancer Res, 58: 2209-16, 1998.
38. ↵
Tonn JC, Kerkau S, Hanke A, et al Effect of synthetic matrix-metalloproteinase inhibitors on invasive capacity and proliferation of human malignant gliomas in vitro. Int J Cancer, 80: 764-72, 1999.
39. ↵
Sternlicht MD, Werb Z Neutrophil elastase and cathepsin G Kreis T Vale R eds. . Extracellular matrix, anchor, and adhesion proteins, 543-5, Oxford University Press Oxford 1999.
40. *Blackwill F, Mantovani A Inflammation and cancer: back to Virchow?. Lancet, 357: 539-45,*
41. ↵
Donà M, Dell'Aica I, Calabrese F, et al Neutrophil restraint by green tea: inhibition of inflammation and associated angiogenesis and pulmonary fibrosis. J Immunol, 170: 4335-41, 2003.
42. ↵
Albert D, Zündorf I, Dingermann T, Müller WE, Steinhilber D, Werz O Hyperforin is a dual inhibitor of cyclooxygenase-1 and 5-lipoxygenase. Biochem Pharmacol, 64: 1767-75, 2002.
43. ↵
Piscitelli SC, Burstein AH, Chaitt D, Alfaro RM, Falloon J Indinavir concentrations and St. John's wort. Lancet, 355: 547-8, 2000.
44. ↵
Marthijssen RH, Verweij J, de Bruijn P, Loos WJ, Sparreboom A Effects of St. John's wort on irinotecan metabolism. J Natl Cancer Inst (Bethesda), 94: 1247-9, 2002.